DIRAC note 2003-09

Determination of the experimental k-factor

Cibrán Santamarina* Christian P. Schütz†

January 6, 2004

Abstract

This note describes the determination of the normalization (k-factor) in the DIRAC experiment taking into account the detector resolutions and inefficiencies.

1 Introduction

The DIRAC experiment at CERN tries to measure the pionium lifetime of the order of femtoseconds (ground-state) with a precision of 10%. The measurement is performed by analyzing the low relative momentum region of $\pi^+\pi^-$pairs which are created in proton target interactions. The main pion pair sources are the $\pi^+\pi^-$pairs from atomic break-up and the time- and space correlated Coulomb pairs. Their production mechanism can be seen in fig.1. Also accidental, $\pi^+\pi^-$pairs from two different proton target interactions are recorded. A further non-desired background is coming from non-Coulomb pairs in which one of the pions originates from the decay of a long lived source.

The production of atoms is proportional to the production of Coulomb pairs. The proportionally constant is known as the **k-factor**.

The DIRAC apparatus influences the reconstruction of the relative momenta distributions (Q) of the produced atomic and Coulomb pairs through multiple scattering, detector resolutions and inefficiencies. Consequently we also adapt the k-factor to these influences determining its experimental value, which is the goal of this note.

The calculation is made using Monte Carlo methods. In a first step atomic and Coulomb pairs are generated in the target. From there the $\pi^+\pi^-$pairs travel through the

*For correspondence:Cibrán Santamarina, CERN 585-R-010, CH-1211 Geneva 23, phone +41 22 767 65 74, email cibran.santamarina.rios@cern.ch.

†For correspondence: Christian Schütz, CERN, 585-R-005, CH-1211 Geneva 23, phone +41 22 767 38 91, email christian.schuetz@cern.ch.

simulated setup and are reconstructed by the offline tracking code. In addition we apply some analysis cuts in order to restrict the sample to time-correlated events with low relative momenta. The so obtained distributions can be compared to the (theoretical) input ones to determine the changes in the k-factor.

This note is structured as follows: Section two explains the underlying theoretical aspects, section three the generator, section four illustrates the Monte Carlo, section five presents results and section six concludes.

2 Theoretical considerations

2.1 Atomic pairs and Coulomb pairs

Let us consider an inelastic collision of one proton from the 24 GeV/c PS beam and a target nucleus. With some probability a $\pi^+\pi^-$pair will be produced. In particular we are interested in those pairs where both pions are produced very close one to each other compared with the range of their Final State Coulomb Interaction (FSI) given by the pionium Bohr Radius ($a_\pi = 387 \times 10^{-15}\ m$). This means we neglect the pions produced from decays of long-lived resonances (e.g. η, K^0_S and Λ) and created far away from the vertex [1], and hence from the other pion of the pair, and keep the $\pi^+\pi^-$pairs in which both pions are created from direct hadronic processes and decays of resonances with a very short lifetime. The yield of this kind of pairs is given by the double inclusive cross section

$$\frac{\mathrm{d}^2\sigma^0_s}{\mathrm{d}\vec{p}\,\mathrm{d}\vec{q}}$$

where $\vec{p}$ and $\vec{q}$ are the π^+ and π^- momenta. The superscript 0 means that FSI has not been considered.

It is well known that in a two particle system we can switch between the coordinates of the particle and the center of mass and relative position coordinates. In particular, the momenta are related by:

$$\vec{P} = \vec{p} + \vec{q} \qquad \vec{Q} = \gamma(\vec{p} - \vec{q})_\parallel + (\vec{p} - \vec{q})_\perp \tag{1}$$

where $\parallel$ stands for the component of $\vec{p} - \vec{q}$ parallel to $\vec{P}$ and $\perp$ for the perpendicular. In particular, for relativistic particles, as those of DIRAC we can assume $\gamma \approx E/M$ where M, is two times de mass of the pion. Thus, any double cross section can be transformed from the pair $\vec{P}$, $\vec{Q}$ to the pair $\vec{p}$, $\vec{q}$ as:

$$\frac{\mathrm{d}^2\sigma}{\mathrm{d}\vec{P}\,\mathrm{d}\vec{Q}} = \frac{E}{M}\frac{\mathrm{d}^2\sigma}{\mathrm{d}\vec{p}\,\mathrm{d}\vec{q}}. \tag{2}$$

The double inclusive cross section has a strong interaction origin. This means that its range of change as a function of the relative momentum is given by the inverse of the strong interaction scale. If we assume $1fm$ for the strong interaction range the cross section will appreciably change if $Q \sim \hbar c/1fm \sim 200MeV$. In the framework

[1] The range of Coulomb interaction between two pions is given by the Bohr radius of pionium, 387.5 fm. The mean free paths of relativistic η, K^0_S and Λ are 1.7 Å, 2.2 cm and 7.89 cm. The η' is the only resonance with a mean free path of the same order as the Bohr radius, 786 fm. However, only 1% of π^- pions are created from its decay [9]. The production of pionic atoms from $\pi^+\pi^-$pairs from the same decay is also posible but tiny [10].

of DIRAC we will only record $\pi^+\pi^-$pairs with $Q < 20MeV/c$. This permits us to consider:

$$\frac{\mathrm{d}^2\sigma_s^0}{\mathrm{d}\vec{p}\,\mathrm{d}\vec{q}} \approx \lim_{\vec{Q}\to 0}\left(\frac{\mathrm{d}^2\sigma_s^0}{\mathrm{d}\vec{p}\,\mathrm{d}\vec{q}}\right). \tag{3}$$

which is correct to better than 2.4% [5].

With a certain probability some of these pion pairs will bind one to each other by means of the Coulomb final state interaction (FSI) leading to pionium, the $\pi^+\pi^-$bound system. The mathematical representation of pionium production is given by the cross section [4]:

$$\frac{\mathrm{d}\sigma_{nlm}^A}{\mathrm{d}\vec{P}} = (2\pi)^3\left|\psi_{nlm}(0)\right|^2\frac{E}{M}\lim_{\vec{Q}\to 0}\left(\frac{\mathrm{d}^2\sigma_s^0}{\mathrm{d}\vec{p}\,\mathrm{d}\vec{q}}\right). \tag{4}$$

where the effect of the final state Coulomb interaction is a bound state with quantum numbers n, l, and m as the squared wave function at the origin reflicts.

Aside from atoms, the Coulomb FSI also leads to an enhancement of $\pi^+\pi^-$ double inclusive cross section for low relative momentum (Q) pairs from short lived sources

$$\frac{\mathrm{d}^2\sigma_s}{\mathrm{d}\vec{P}\,\mathrm{d}\vec{Q}} = A_C(Q)\frac{E}{M}\frac{\mathrm{d}^2\sigma_s^0}{\mathrm{d}\vec{p}\,\mathrm{d}\vec{q}}\,; \qquad A_C(Q) = \frac{2\pi M_\pi\alpha/Q}{1-\mathrm{e}^{-2\pi M_\pi\alpha/Q}}\,, \tag{5}$$

$A_C(Q)$ has a pole at zero and tends to one for large Q. This means that low Q pairs are bent into even lower relative momentum while large relative momentum pairs are only slightly affected by the FSI.

Taking (3) into account we can approximate:

$$\frac{\mathrm{d}^2\sigma_s}{\mathrm{d}\vec{P}\,\mathrm{d}\vec{Q}} \approx A_C(Q)\frac{E}{M}\lim_{Q\to 0}\left(\frac{\mathrm{d}^2\sigma_s^0}{\mathrm{d}\vec{p}\,\mathrm{d}\vec{q}}\right). \tag{6}$$

which is the analogue of equation (4) for the production of not bound states. The analogy is complete if we notice that the Coulomb enhancement factor $A_C(Q)$ can be written as

$$A_C(Q) = (2\pi)^3\left|\psi_{\vec{Q}}^{(+)}(0)\right|^2 \tag{7}$$

where the $\psi_{\vec{Q}}^{(+)}(\vec{r})$ are a particular complete set of solutions of the continuum spectrum with the characteristic of asymptotically becoming an outgoing plane wave with $\vec{Q}$ momentum. This set of solutions was obtained by A. Sommerfeld and this is why they are sometimes referred to as the Sommerfeld wave functions.

Dividing equations (4) and (6) we eliminate the laboratory momentum dependence and calculate the relative yield between Atoms and Coulomb pairs. Integrating (6) in a region of the phase space, Ω, the ratio between the number of created atoms (N^A), created in any bound state, and the number of Coulomb pairs (N^{Coul}) holding $\vec{Q}\in\Omega$ is [2]:

$$\text{k-factor} = \frac{N^A}{N^{Coul}(\vec{Q}\in\Omega)} = \frac{\displaystyle\sum_{nlm}\frac{\mathrm{d}\sigma_{nlm}^A}{\mathrm{d}\vec{P}}}{\displaystyle\int_{\vec{Q}\in\Omega}\frac{\mathrm{d}\sigma_s^C}{\mathrm{d}\vec{P}\mathrm{d}\vec{Q}}\mathrm{d}\vec{Q}} = \frac{(2\pi)^3\displaystyle\sum_{nlm}\left|\psi_{nlm}(0)\right|^2}{\displaystyle\int_{\vec{Q}\in\Omega}A_C(Q)\mathrm{d}\vec{Q}} \tag{8}$$

[2]The effect of the strong interaction between the two pions changes the Coulomb factor and the atomic wave function by the same multiplicative factor which is also suppressed when the ratio for the k-factor is calculated [6].

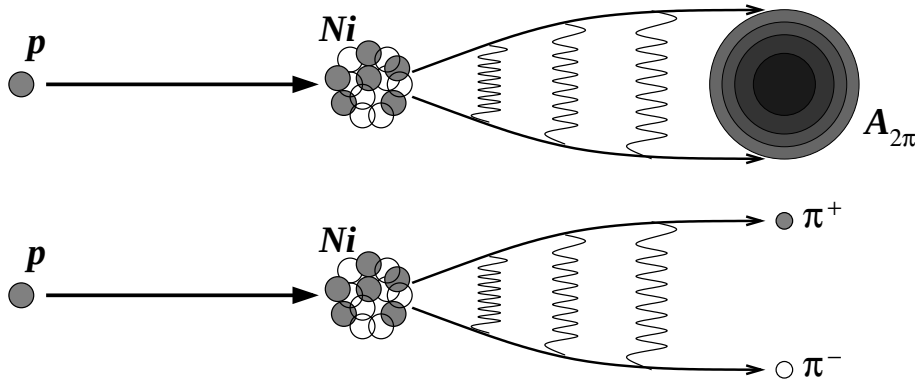

Figure 1: This figure shows the parallel production mechanism of atomic bound states (top) and free $\pi^+\pi^-$ Coulomb pairs (bottom).

Ω_1	K_Q	$\Omega_2(Q_T < 4.)$	K_{Q_l}
$Q < 1.$	2.493	$Q_l < 1.$	0.252
$Q < 1.5$	1.104	$Q_l < 1.5$	0.174
$Q < 2.$	0.615	$Q_l < 2.$	0.134
$Q < 2.5$	0.387	$Q_l < 2.5$	0.111
$Q < 3.$	0.263	$Q_l < 3.$	0.094
$Q < 3.5$	0.188	$Q_l < 3.5$	0.083
$Q < 4.$	0.140	$Q_l < 4.$	0.074
$Q < 4.5$	0.107	$Q_l < 4.5$	0.067
$Q < 5.$	0.084	$Q_l < 5.$	0.061

Table 1: K factor value, according to equation (8) for two different choices of Ω. All relative momentum values are in MeV/c.

In Table 1 and Figure 2 we show the value of the K factor for two particular Ω choices, $\Omega_1 = \{$events with $Q < Q^0\}$ and $\Omega_2 = \{$events with $Q_T < 4\ MeV/c$ and $Q_l < Q_l^0\}$.

2.2 Coulomb and Non Coulomb pairs

In addition to atomic and Coulomb correlated pairs also Non Coulomb $\pi^+\pi^-$ pairs are detected in the framework of the DIRAC experiment. These are time correlated pairs, and hence both pions come from the same proton-target interaction, where at least one of the pions is produced in the decay of a long lived particle. The production mechanism is schematically shown in Figure 3.

The total production of time correlated $\pi^+\pi^-$ pairs is given by the short lived and long lived sources. The proportion of pion pairs produced by long lived sources (ω_l) has been shown to depend only on P [8], the magnitude of the total momentum of the pair. Hence we can write the production cross section for this type of pairs as:

$$\frac{\mathrm{d}^2\sigma_l}{\mathrm{d}\vec{p}\mathrm{d}\vec{q}} = \omega_l(P)\frac{\mathrm{d}^2\sigma}{\mathrm{d}\vec{p}\mathrm{d}\vec{q}} \tag{9}$$

where $\mathrm{d}^2\sigma/\mathrm{d}\vec{p}\mathrm{d}\vec{q}$ is the double differential inclusive total cross section (no matter

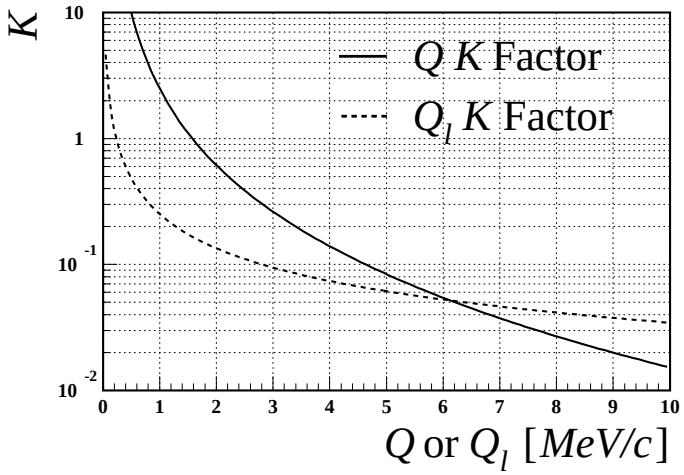

Figure 2: K factor value at the generation point. The Q_l value has a cut on $Q_T < 4MeV/c$.

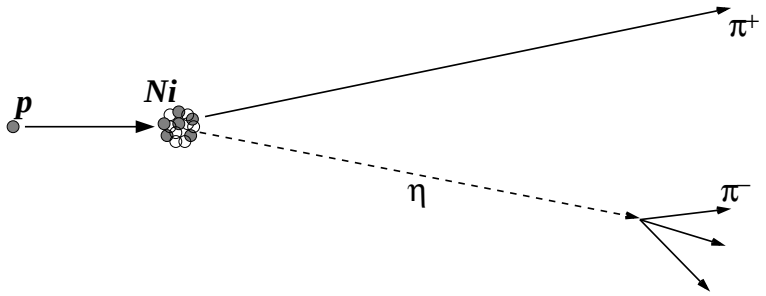

Figure 3: Production mechanism of non-Coulomb pairs.

wether short or long lived sources). It can be obtained after the acceptance cuts of DIRAC spectrometer from the experimental prompt events data. We have obtained $\omega_l(P)$ using pure FRITIOF6 Monte Carlo distributions [11].

Knowing $\mathrm{d}^2\sigma/\mathrm{d}\vec{p}\mathrm{d}\vec{q}$ and $\omega_l(P)$ we can also obtain the double inclusive cross section from short-lived sources:

$$\frac{\mathrm{d}^2\sigma_s}{\mathrm{d}\vec{p}\mathrm{d}\vec{q}} = (1-\omega_l(P))\frac{\mathrm{d}^2\sigma}{\mathrm{d}\vec{p}\mathrm{d}\vec{q}} \tag{10}$$

which is needed for the Atomic and Coulomb pair generators.

The previous discussion is only the starting point for the determination of the number of produced atomic pairs by studying the measured low relative momentum background. This is because due to the multiple scattering in the target and the performance of the DIRAC spectrometer, the final measured relative momentum distribution is different from the one at the generation point. This affects both types of pairs, atomic and Coulomb ones, but not necessarily equally.

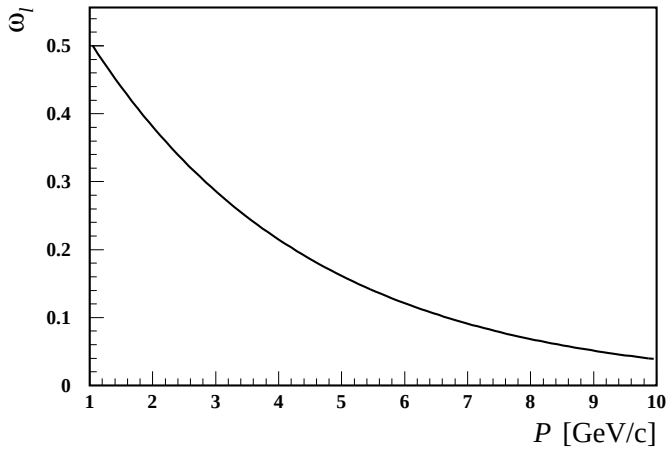

Figure 4: The ratio of pion pairs from long lived sources $\omega_l(P)$.

3 Generator

As a pion pair is a system of two particles six degrees of freedom have to be determined to completely specify its state. Also the position of the center of mass has to be generated.

We have chosen our set of variables to be the laboratory center of mass and the relative momentum polar coordinates (P, θ, ϕ) and (Q, θ', ϕ'), see Figure 5.

We have used experimental input for the laboratory Center of Mass momentum. As equations (4) and (6) depend on the cross section at $Q = 0$ we have applied a cut on $Q < 5MeV/c$. We have checked that the cross section does not change more than 2% (mean value) if we compare it to its analogue with the $5MeV/c < Q < 10MeV/c$ cut. The measured two dimensional spectrum of time correlated events, as a function of P and θ, has been divided by the spectrometer acceptance. The latter has been calculated using the Monte Carlo simulation of the detector (GEANT-DIRAC) [3] [16]. The resulting distribution has been multiplied by $(1 - \omega_l(P))$ to suppress the contribution from long lived sources. The ϕ angle is independent due to the axial symmetry of the proton target interaction. Figure 6 displays the momentum distribution of pion pairs from short lived sources (Coulomb and Atomic pairs) before and after the acceptance correction.

3.1 Atomic Pair Generator

The most complete version of the atomic pair generator is described in [14]. The laboratory momentum (P, θ) are generated according to the 2-dimensional leftmost distribution of Figure 7, obtained as described above, while ϕ is generated according to rightmost plot of the same Figure 7.

[3] For the acceptance calculation we have used a uniform (P, θ) distribution with soft geometric cuts.

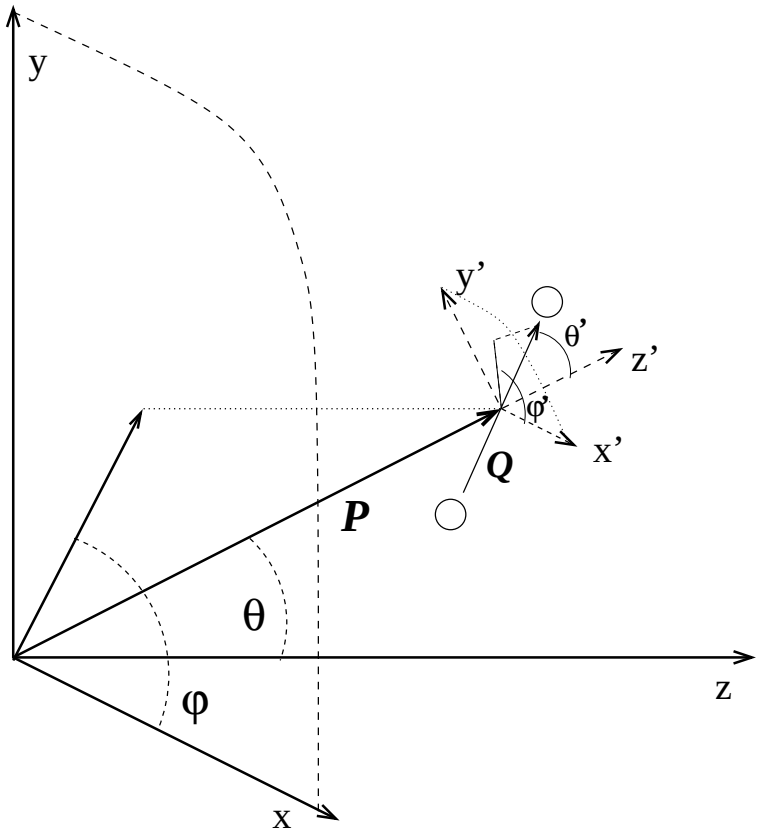

Figure 5: Description of the coordinates used for the pions pairs generators.

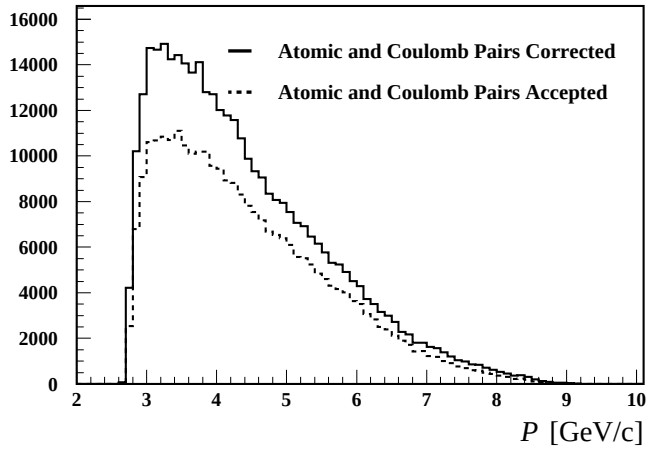

Figure 6: Coulomb and Atomic pairs laboratory momentum distributions after detection (dashed) and corrected for the acceptance (solid).

The Z coordinate, which corresponds to the position in the target depth where the atomic pair is produced (a dissociation happens), is generated according to the distribution shown in Figure 7 obtained from the complete Monte Carlo [14]. Atomic pairs are produced from the break-up of a bound state which has flown away a certain distance from the primary proton-target production vertex. The primary vertexes are uniformly distributed along the target since the nuclear interaction length is several centimeter (much larger than the target thickness of several tenths of microns). This explains that the Z distribution goes to zero at the target beginning.

The X and Y distributions are given by the beam transverse gaussian profile with $\sigma_X = 1mm$ and $\sigma_Y = 1.5mm$ [2].

The relative momentum is generated according to the scheme:

- Once the break-up position is determined we select a father state for the broken atom. This selection is made according to the distribution of Figure 8 which is obtained from the Monte Carlo of [14]. The m number of the bound state is unimportant for the relative momentum generation [15].
- If the father state is the $1S$ or the $2S$ bound state we generate Q, the magnitude of the relative momentum, according to the distributions obtained in [7]:

$$\frac{d\sigma^{1S}}{dQ} \propto \frac{\frac{Q}{M_\pi \alpha}}{\left[\left(\frac{Q}{M_\pi \alpha}\right)^2 + 1\right]^5} \frac{\exp\left[-\frac{4M_\pi \alpha}{Q} \tan^{-1} \frac{Q}{M_\pi \alpha}\right]}{\left[1 - \exp\left(-\frac{2\pi M_\pi \alpha}{Q}\right)\right]}, \tag{11}$$

$$\frac{d\sigma^{2S}}{dQ} \propto \frac{\frac{Q}{M_\pi \alpha}\left[\left(\frac{Q}{M_\pi \alpha}\right)^2 + 1\right]}{\left[4\left(\frac{Q}{M_\pi \alpha}\right)^2 + 1\right]^6} \frac{\exp\left[-\frac{4M_\pi \alpha}{Q} \tan^{-1} \frac{2Q}{M_\pi \alpha}\right]}{\left[1 - \exp\left(-\frac{2\pi M_\pi \alpha}{Q}\right)\right]}, \tag{12}$$

while if $n > 2$ we use equation (11) where instead of Q we have $Q/2n$ as suggested in [15].

The polar angle θ' is generated according to a $\sin^{2l+1}\theta'$ distribution [15] and ϕ' is generated according to a uniform distribution in the $(0, 2\pi)$ interval.

3.2 Coulomb Pair Generator

A main difference between Atomic and Coulomb pairs concerns the position of the pair generation. Coulomb pairs are generated nearby the primary vertex where the proton-target takes place. This means the generation position is uniformly distributed along the target thickness while the transverse coordinates follow the beam profile as for the case of Atomic pairs.

The generation of Coulomb Pair momenta is made according to equation (6). This means that $\vec{P}$ is treated exactly in the same way as for atomic pairs. The $\vec{Q}$ values are generated according to:

$$\frac{d\sigma^{Coul}}{dQ} = \frac{2\pi M_\pi \alpha / Q}{1 - \mathrm{e}^{-2\pi M_\pi \alpha / Q}} Q^2 \tag{13}$$

which is the Coulomb correlation function times the Q^2 factor of the phase space element $d\vec{Q}$.

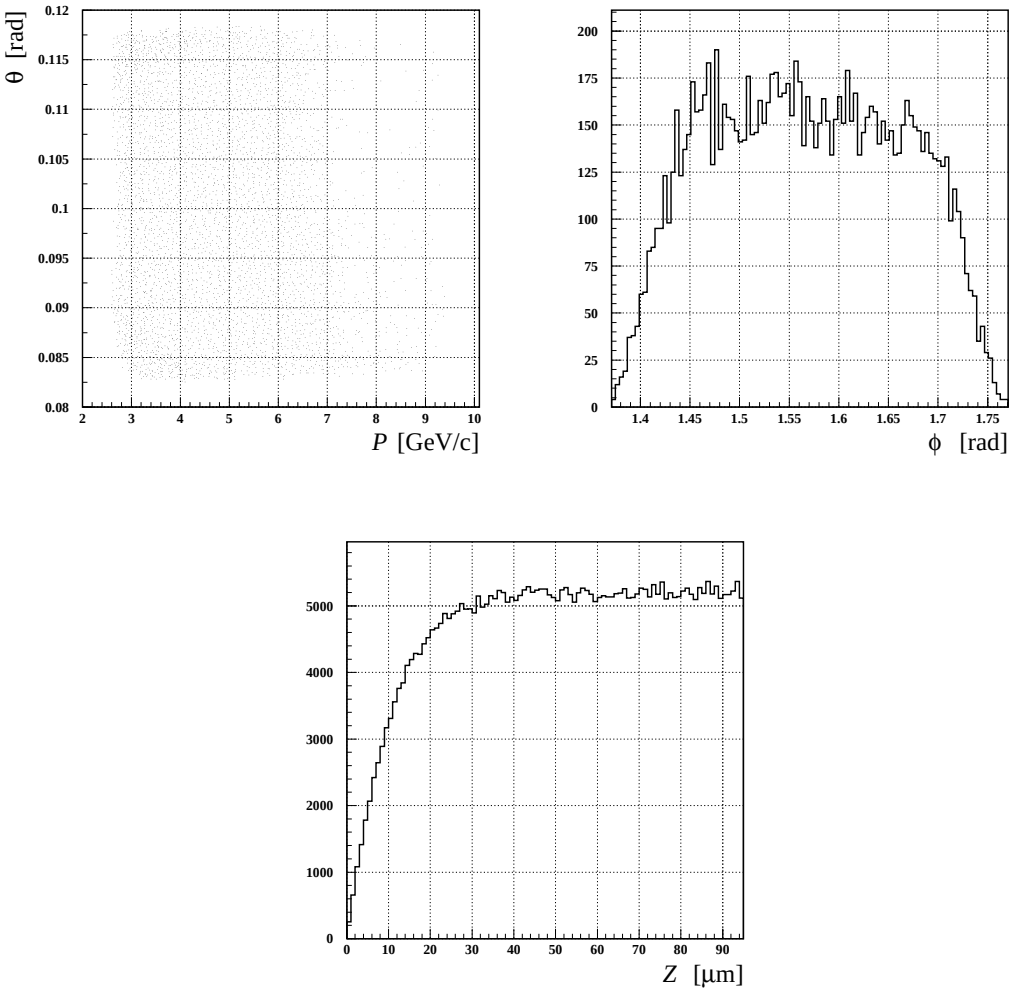

Figure 7: Input distributions for the (P, θ) (top left) and ϕ generation of Atomic and Coulomb pairs. The bottom distribution is used to generate the break-up position of atoms in the target.

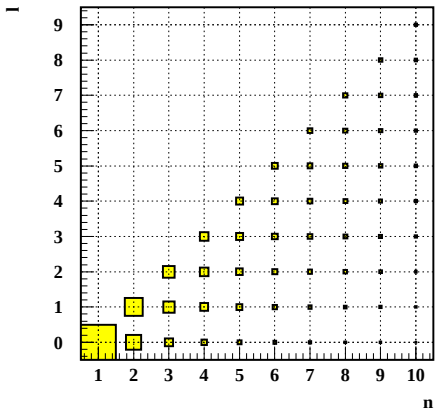

Figure 8: Correlated distribution of principal n and angular l quantum numbers at break-up.

The θ' angle is given by the phase space element only:

$$\frac{d\sigma^{Coul}}{d\theta'} = \sin\theta' \tag{14}$$

whereas ϕ' is uniformly random in the $(0, 2\pi)$ range.

4 Monte Carlo (GEANT)

Our Monte Carlo (GEANT-DIRAC) is based on GEANT [16]. The complete DIRAC setup is simulated including the trigger and the detector digitalization. A precise description of the detector simulation can be found in [17]. The GEANT-DIRAC output is processed by the offline reconstruction program ARIANE[18] in the same way as experimental data. In this analysis we use the BASEL tracking algorithm [19].

The simulated events have been generated according to the measured absolute momentum spectrum taking into account the detection efficiency.

A detailed study of the response of the DIRAC detector to simulated events can be found in an earlier note [20]. In this note we put particular emphasis on the upstream scintillation fiber tracking detector (SFD), since it is essential for the determination of the relative momentum projections. It is crucial to the relative momentum determination since the distance between two tracks at the level of SFD X and Y translates directly into a Q_x and a Q_y. The SFD simulation has been tuned for the 94 / 98 μm thick Ni targets separately. Figure 9 shows the difference in selected fibers for the tracking for 94μm target size real data (black) recorded in 2001 and Monte Carlo data (red) for the SFD X (right plot) and the SFD Y plane (left plot). The data was selected with a cut on reconstructed Q_{trans} <4MeV/c and $|Q_{long}|$ <10 MeV/c. In addition we restrict the sample to two hit fiber candidates in the SFD detector in order to reduce ambiguities on the hit assignment. The two plots show good agreement between experimental data and Monte Carlo.

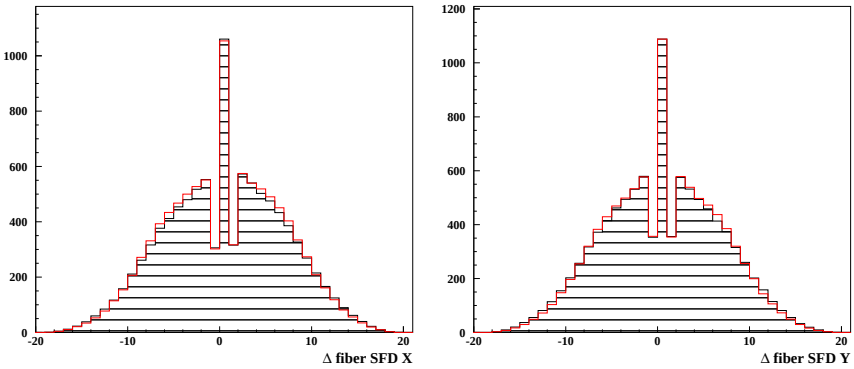

Figure 9: Difference of hit fibers chosen by the tracking for experimental data (black) and Monte Carlo Coulomb pair events (red) for Ni 94μm 2001 data in the X (left) and Y layer (right) of the SFD.

5 Experimental k-factor

5.1 Calculation

The theoretical k-factor (k^{th}) from equation 8 relates the number of produced atoms (N_i^A) to the number of produced Coulomb pairs (N^{Coul}) at production. The experimental value of the k-factor (k^{exp}) is different from the theoretical one because of multiple scattering in the target and in the setup, because of geometrical acceptance, trigger, detector and tracking inefficiencies. We define the breakup probability P_{br} as the number of broken up atoms (n_i^A) to the number of produced atoms (N_i^A). The latter can be replaced with the number of produced Coulomb pairs multiplied with the k-factor. As a result we can write:

$$P_{br} = \frac{n_i^A}{N_i^A} = \frac{n_i^A}{k^{th} \cdot N^{Coul}(Q^{initial} < 2)} \tag{15}$$

n_i^A,N_i^A and N^{Coul} are defined at production, where the subscript i stands for 'initial'. The Coulomb pairs considered have an initial Q of less than 2 MeV/c which corresponds to the Q range of the atomic pairs. By considering Coulomb pairs only for Q less than 2 MeV/c we make sure that the reconstruction efficiency is comparable for atomic and Coulomb pairs.

The measurement on the other hand yields the number of reconstructed atomic ($n^A(Q^{rec} < Q^{cut})$) and Coulomb pairs ($N^{Coul}(Q^{rec} < Q^{cut})$) below a certain Q^{cut}. We can relate these measured values to the ones at production in the following way

$$\frac{n_i^A}{k^{th} \cdot N^{Coul}(Q^{init} < 2)} \stackrel{!}{=} \frac{n^A(Q^{rec} < Q^{cut})}{k^{exp} \cdot N^{Coul}(Q^{rec} < Q^{cut})} \tag{16}$$

to yield an equation for the the experimental k-factor, k^{exp} as a function of the relative (cut) momentum Q^{cut}:

$$k^{exp}(Q^{cut}) = k^{th} \frac{n^A(Q^{rec} < Q^{cut})}{n_i^A} \frac{N^{Coul}(Q^{init} < 2)}{N^{Coul}(Q^{rec} < Q^{cut})} \tag{17}$$

The same methodology can also be applied to Q_l to yield:

$$k^{exp}(Q_l^{cut}) = k^{th}\frac{n^A(Q_l^{rec} < Q^{cut})}{n_i^A}\frac{N^{Coul}(Q^{init} < 2)}{N^{Coul}(Q_l^{rec} < Q^{cut})} \tag{18}$$

The above equations 17 and 18 show that the experimental k-factor can be regarded as the theoretical one after taking into account the reconstruction probabilities for Coulomb and atomic pairs. To illustrate this, consider for example equation 18. We can define the probability of reconstructing an atomic pair below a given cut as:

$$\frac{n^A(Q_l^{rec} < Q^{cut})}{n_i^A} = P_A(Q^{cut}) \tag{19}$$

In analogy we can define the probability of reconstructing a Coulomb pair below a given cut from an initial sample of $Q^{init} < 2$ MeV/c as

$$\frac{N^{Coul}(Q_l^{rec} < Q^{cut})}{N^{Coul}(Q^{init} < 2)} = P_{Coul}(Q^{cut}) \tag{20}$$

The experimental k-factor from equation 18 becomes then

$$k^{exp}(Q^{cut}) = k^{th}\frac{P_A(Q^{cut})}{P_{Coul}(Q^{cut})}$$

In short we can calculate the breakup probability from the measured Coulomb and atomic pairs according to the following equation 21

$$P_{br} = \frac{n^A(Q^{rec} < Q^{cut})}{k^{exp} \cdot N^{Coul}(Q^{rec} < Q^{cut})} \tag{21}$$

5.2 Results for Nickel 2001

For the Nickel 2001 data we evaluate k^{exp} for two target thicknesses: 94 and 98 μm. We require the events to pass a time correlation in the two arms of the vertical hodoscopes of $|dt_{VH}| < 0.5$ ns. In addition we accept only events with a maximum of two good hits[4] per SFD plane (to remove hit assignment ambiguity, hence suppressing background) and low $Q's$:

$$|Q_{trans}| < \text{ 4 MeV/c and } |Q_{long}| < \text{ 10 MeV/c} \tag{22}$$

5.2.1 94 μm target

Table 2 shows the result for the 94 μm target case. The experimental k-factors are calculated using a Monte Carlo sample of 15 Mio events for Coulomb pairs and 600 thousand events for atomic pairs. The size of the sample explains the very small statistical error on the resulting values. The errors have been calculated using binomial error theory[5].

[4]The definition of good hits in the SFD can be found in [19]. Stated simply, we require the hit fibers to be time correlated with the reconstructed track in the drift chambers as well as within a geometrical tracking window.

[5]We assume a binomial distribution. The Variance is then given by $V(r) = E(r^2) - (E(r))^2 = n(n-1)p^2 + np - (np)^2 = np(1-p)$ where n denotes number of trials and p the probability of a success. More details can be found in [26].

	n^A	N^{Coul}	k^{exp}
Total produced	599267	14892663	
Produced with $Q^{init} < 2$ MeV/c	594799	315568	
$Q^{Rec} < 2$ MeV/c	105451±124	61694±16	0.5535±0.0007
$Q^{Rec} < 3$ MeV/c	125913±145	158948±41	0.2565±0.0003
$Q^{Rec} < 4$ MeV/c	131300±150	307297±79	0.1384±0.0002
$Q_l^{Rec} < 1$ MeV/c	120872±140	128173± 33	0.3054±0.0004
$Q_l^{Rec} < 2$ MeV/c	130217±149	237736± 61	0.1774±0.0002

Table 2: Detected Coulomb and atomic pairs for the 94 μm target for reconstructed Q and Q_l after setup acceptance, trigger and reconstruction efficiencies, time and analysis cuts. Using equation 17 and the known input factors n_i^A= 599267 and $N^{Coul}(Q^{init} < 2)$= 315568, the experimental k-factor can be calculated in dependence on the reconstructed relative momentum.

5.2.2 98 μm Target

Table 3 shows the result for the 98 μm target case. The results for the experimental k-factor differ slightly from the ones for the 94 μm target. The reason for this difference can be attributed to a different SFD response and a slightly bigger multiple scattering than in the 98 μm case.

	n^A	N^{Coul}	k^{exp}
Total produced	599252	14947054	
Produced with $Q^{init} < 2$ MeV/c	594711	316481	
$Q^{Rec} < 2$ MeV/c	102005±120	60483 ± 16	0.5478±0.0007
$Q^{Rec} < 3$ MeV/c	122853±142	156118± 40	0.2556±0.0003
$Q^{Rec} < 4$ MeV/c	128286±147	301222± 77	0.1383±0.0002
$Q_l^{Rec} < 1$ MeV/c	117731±137	125627± 32	0.3044±0.0003
$Q_l^{Rec} < 2$ MeV/c	127242±146	232647± 60	0.1776±0.0002

Table 3: Detected Coulomb and atomic pairs for the 98 μm target for reconstructed Q and Q_l after setup acceptance, trigger and reconstruction efficiencies, time and analysis cuts. Using equation 17 and the known input factors n_i^A= 599252 and $N^{Coul}(Q^{init} < 2)$= 316481, the experimental k-factor can be calculated in dependence on the reconstructed relative momentum.

6 Systematic influences

The evaluation of the experimental k-factor should also consider systematic influences. In this section we examine how a change of the multiple scattering of 5% influences the experimental k-factors.

In order to study this effect, we increase (decrease) the multiple scattering angle calculated by GEANT by 5%. Then we redo the above explained analysis. Because the statistical errors are very small[6] a systematic influence can become easily dominant.

[6]Especially as compared to the error of the DIRAC measurement, which is of the order of 5%.

First we can compare the influence of changing the multiple scattering on the background. For this study we use the reconstruction probabilities for Coulomb, $P_{Coul}(Q^{cut})$, and for atomic pairs, $P_A(Q^{cut})$, as defined above in equation 19 and 20 and calculate the relative changes of these probabilities due to a change in the multiple scattering:

$$\Delta P_j(Q^{cut}) = \frac{P_j(Q^{cut})|_{\text{MS}\pm 5\%} - P_j(Q^{cut})|_{\text{standard MS}}}{P_j(Q^{cut})|_{\text{standard MS}}} \quad j = A, Coul \qquad (23)$$

Figure 10 illustrates the changes to the background for both Coulomb and atomic pairs (in percent). The atomic pairs are more affected by a change in the multiple scattering than the Coulomb pairs, especially for low Q values. The Coulomb pair

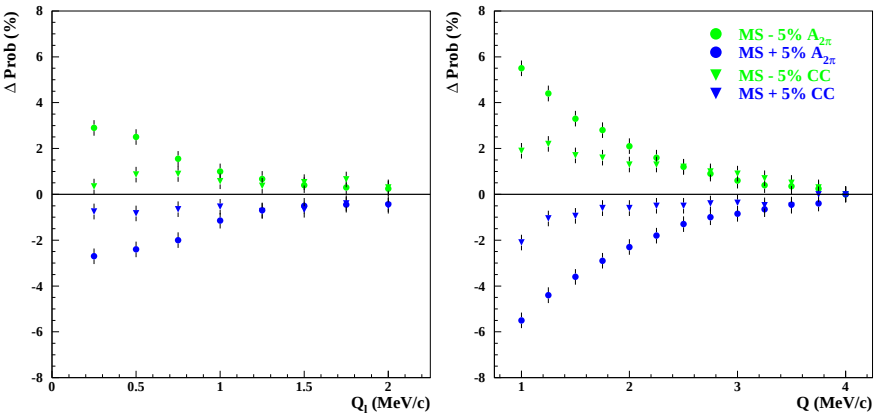

Figure 10: Change in the background in Q_l and Q for Coulomb and atomic pairs as defined in equation 23 for increasing and decreasing the multiple scattering by 5%.

background seems to be stable down to $Q = 1.5$ MeV/c and $Q_l = 0$ MeV/c with a little effect for smaller Q values. In addition, the Coulomb pairs seem to be slightly asymmetric in Q. The atomic pair on the other hand change their shape in the total Q spectrum up to 4 MeV/c. The effect becomes very dominant for $Q < 2$ MeV/c. The effect for the atomic pairs is more symmetric than for the Coulomb pairs. It is more pronounced in Q than in Q_l. We expect these changes (especially the atomic pairs) to influence the experimental k-factor.

Table 4 (5) displays the results obtained for the 94 μm target increasing (decreasing) the multiple scattering angle by 5%. We notice that increasing (or decreasing) the multiple scattering of 5% introduces a negliable effect for $Q^{Rec} < 4$ MeV/c and $Q_l^{Rec} < 2$ MeV/c, while an important change is found for smaller cut, i.e. $Q^{Rec} < 2$ MeV/c and $Q_l^{Rec} < 1$ MeV/c. Since the pionic atom signal extends up to 4 MeV in Q and up to 2 MeV in Q_l, we have to take this source of systematic error into account when cutting into the signal.

We can define an error on the experimental k-factor by calculating the percentage difference in the k-factor value of the standard and the increased (decreased) multiple scattering (MS):

$$\Delta k^{exp} = \frac{k^{exp}(\text{MS} \pm 5\%) - k^{exp}(\text{standard MS})}{k^{exp}(\text{standard MS})} \qquad (24)$$

	n^A	N^{Coul}	k^{exp}
Total produced	599237	9592560	
Produced with $Q^{init} < 2$ MeV/c	594783	203206	
$Q^{Rec} < 2$ MeV/c	103267±122	39979±13	0.5387±0.0007
$Q^{Rec} < 3$ MeV/c	125821±145	103030±33	0.2547±0.0003
$Q^{Rec} < 4$ MeV/c	132064±151	199359±64	0.1382±0.0002
$Q_l^{Rec} < 1$ MeV/c	120577±140	83079± 27	0.3027±0.0004
$Q_l^{Rec} < 2$ MeV/c	130911±150	154088± 49	0.1772±0.0002

Table 4: Detected Coulomb and atomic pairs for the 94 μm target after **increasing** the multiple scattering angle by 5%. The table shows the resulting values for reconstructed Q and Q_l after setup acceptance, trigger and reconstruction efficiencies, time and analysis cuts. Using equation 17 and the known input factors n_i^A= 599237 and $N^{Coul}(Q^{init} < 2)$= 203206, the experimental k-factor can be calculated in dependence on the reconstructed relative momentum.

	n^A	N^{Coul}	k^{exp}
Total produced	599234	13038438	
Produced with $Q^{init} < 2$ MeV/c	594917	276758	
$Q^{Rec} < 2$ MeV/c	109365±128	55666±15	0.5580±0.0007
$Q^{Rec} < 3$ MeV/c	128217±147	142574±39	0.2554±0.0003
$Q^{Rec} < 4$ MeV/c	132918±152	273715±75	0.1379±0.0002
$Q_l^{Rec} < 1$ MeV/c	123243±140	114473± 32	0.3058±0.0004
$Q_l^{Rec} < 2$ MeV/c	131806±150	211720± 58	0.1768±0.0002

Table 5: Detected Coulomb and atomic pairs for the 94 μm target after **decreasing** the multiple scattering angle by 5%. The table shows the resulting values for reconstructed Q and Q_l after setup acceptance, trigger and reconstruction efficiencies, time and analysis cuts. Using equation 17 and the known input factors n_i^A= 599234 and $N^{Coul}(Q^{init} < 2)$= 276758, the experimental k-factor can be calculated in dependence on the reconstructed relative momentum.

The resulting kfactors and errors are illustrated for Q (upper plots) and Q_l (lower plots) in figure 11 as the blue triangles (green rectangles) for 5% bigger (smaller) multiple scattering. The relative difference is plotted in percent and as a function of the cut momentum in Q and Q_l. The statistical uncertainties of the calculated experimental k-factor value for standard multiple scattering are drawn as a magenta band.

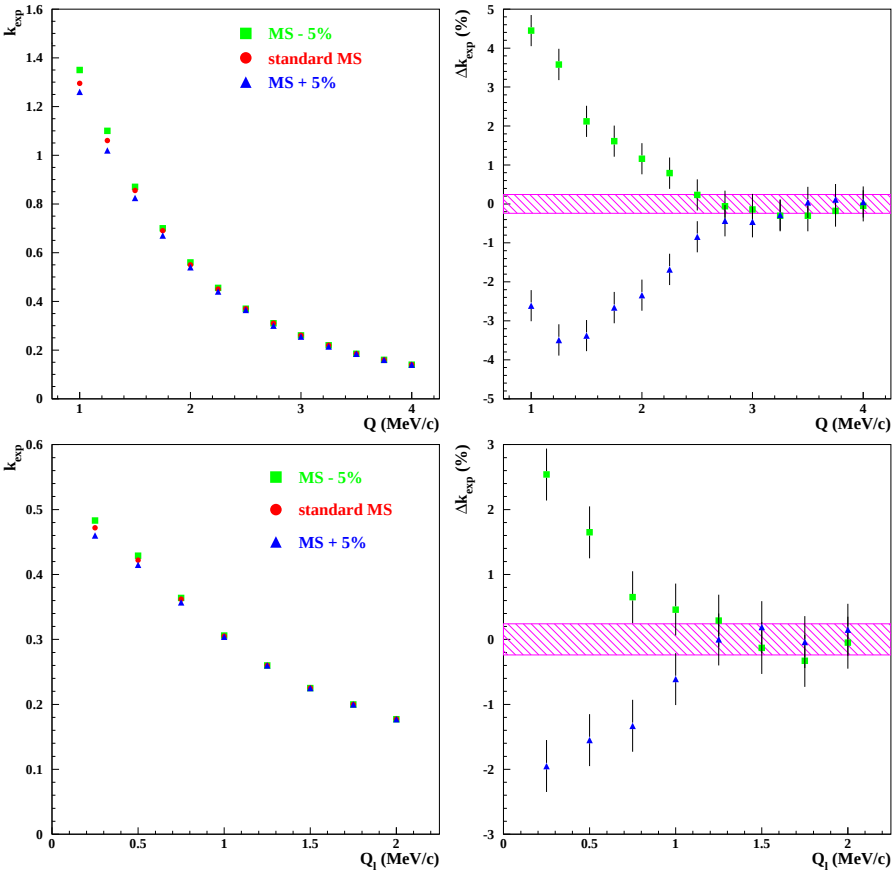

Figure 11: The upper left plot shows the k-factor for standard (red circles), 5% bigger (blue triangles) and 5% smaller (green rectangles) multiple scattering for a cut at Q. The relative change for bigger (and smaller) multiple scattering with respect to the standard case (in percent) is drawn in the right upper plot. The magenta band illustrates the error due to statistical uncertainty of the k-factor. The lower two plots show the k-factor (left) and the relative change for a cut at Q_l.

The figures illustrate how much the low Q (Q_l) region is affected by a change in multiple scattering. If we apply a strong cut on Q (i.e. $Q < 1.5$ MeV/c) to extract the signal, we induce an uncertainty in the k-factor which can become comparable to the expected measurement uncertainty in the experimental data (which is around 5%). In contrast, if we accept most of the pionium signal (which extends up to 4 MeV/c), the error induced due to the multiple scattering is comparable to the statistical uncertainty and about two orders of magnitude smaller than the error arising from the measurement. The asymmetric behavior of Δk^{exp} for increasing versus decreasing the multiple scattering is not caused by a different normalization (since we divide in

equation 24 for bigger and smaller multiple scattering alike by the same value), but by the sensitivity of the Coulomb pairs to the multiple scattering change for very small Q's. Decreasing the multiple scattering by 5% increases the amount of Coulomb pairs for small Q's more than their amount is decreased by increasing the multiple scattering. On the other hand, the effect of increasing versus decreasing the multiple scattering is symmetric for atomic pairs, which explains the observed asymmetry in Δk^{exp}.

7 The k-factor in a simplified toy model

We have studied the possibility to obtain the k-factor, and in addition the histograms with the shape of the different types of pairs, by making a modification of the event generator, described in section 3 trying to reproduce the effect of the spectrometer and the tracking algorithm. For that we propagate the Coulomb or atomic after break-up pion pair through the target, the Mylar window of the vacuum chamber and the MSGC detectors accounting for the multiple scattering described with the Moliere theory [16] and we check the distance at the level of the Scintillating Fiber detector. As explained in section 5 the shape of the difference in hit fibers with its enhancement at zero and the dips at ± 1 is due to the readout electronics of the detector and to the single hit inefficiency. Thus, the performance of this detector is a major ingredient of the Q_x and Q_y distorsion and must be taken into account. To reproduce the SFD distributions we have used the next algorithm:

- We have independently checked which is the difference between the hit fibers at X and Y plane.
- We have suppresed with 5% probability per plane one of the hits and set the fiber distance at zero. Therefore these events populate the central peak.
- If the difference was ± 1 we have randomly chosen an amount of events to decrease the statistic on the corresponding bin to the experimental value and also set the corresponding fiber difference in the X and Y plane to zero.
- We have suppresed the excess of events at the X and Y peaks taking care that the laboratory momentum spectrum is not distorted [7].

The corresponding Δ_x and Δ_y distributions in the SFD detector are compared to the Monte Carlo results used as pattern in figure 12 for a sample of Coulomb pairs.

The final reconstructed momentum is simulated by jittering the relative momentum components Q_x, Q_y and Q_l after multiple scattering in the target by corresponding gaussian distributions with $\sigma_{Q_x} = \sigma_{Q_y} = 0.45 MeV/c$ and $\sigma_{Q_l} = 0.57 MeV/c$. An exception corresponds to those events shifted to the peak in the SFD which are considered to have initial $Q_x = 0$ or $Q_y = 0$. The resulting spectra for Q and Q_l can be seen in figure 13 while the k-factor results are shown in table 6.

We would like to remark that the use of folding or simple toy models has serious disadvantages with respect to the full Monte Carlo. Without the full Monte Carlo we are never sure of the spectra shapes for Coulomb or Atomic pairs below $Q < 3 MeV/c$. After all, our goal was to reproduce the Monte Carlo distributions which should be already available and hence would have no sense not to use them for the

[7] This is extremely important, since the multiple scattering mean angle depends on the laboratory momentum of the particle. Hence, distorting the laboratory momentum spectrum by tunning the Δ_x or Δ_y profile can bias the Q_x and Q_y distributions.

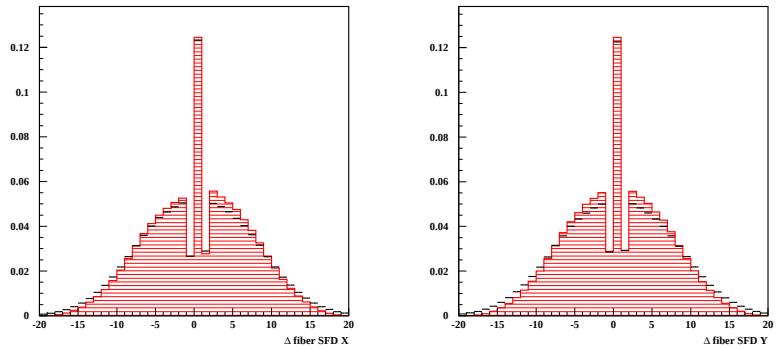

Figure 12: Difference of hit fibers in the toy model (black) and Monte Carlo Coulomb pair events (red) for Ni 94μm 2001 data in the X (left) and Y layer (right) of the SFD.

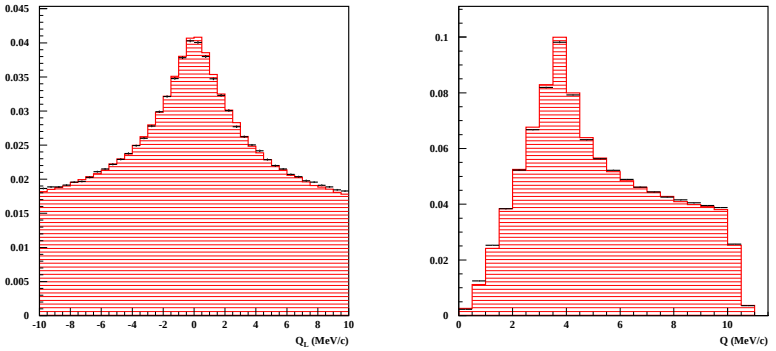

Figure 13: Comparison of the Q and Q_l spectra obtained with the toy model (black) and with the Monte Carlo Coulomb pair events (red) for Ni 94μm 2001 data.

	n^A	N^{Coul}	k^{exp}
Total produced	1000000	10000000	
Produced with $Q^{init} < 2$ MeV/c	997633	96422	
$Q^{Rec} < 2$ MeV/c	711293	81711	0.517 $\pm$0.002
$Q^{Rec} < 3$ MeV/c	849153	205833	0.2452$\pm$0.0006
$Q^{Rec} < 4$ MeV/c	883957	393558	0.1335$\pm$0.0003
$Q_l^{Rec} < 1$ MeV/c	793773	162956	0.2895$\pm$0.001
$Q_l^{Rec} < 2$ MeV/c	882712	303420	0.1729$\pm$0.0004

Table 6: Toy model k-factor results for the 94 μm Ni target tunned for the 2001 Coulomb Monte Carlo pairs.

full analysis of the data and the k-factor determination. Our experience shows that for arbitrary reasonable values of the resolution the folding method can lead to misleading

results with good agreements for $Q \gtrsim 3MeV/c$ but bigg disagreements for lower Q. This is due to the fact that detector performance effects, as the merging of hits or the single hit efficiency, together with the tracking features, like the mismatching of events with two close hits, can not be completly described by simple gaussian jitter of the $\vec{Q}$ components.

8 Conclusion

We have developed a generator for atomic and Coulomb pairs for the DIRAC experimental conditions. The transport of atoms is solved using Monte Carlo, which is the basis of the atomic pair generation. The atomic pairs emerge from a break-up of pionium, their spectrum given by quantum mechanics. The Coulomb pairs' relative momentum distributions are generated according to the Coulomb enhancement function and phase space. Since atoms and Coulomb pairs are both produced from low relative momentum $\pi^+\pi^-$pairs coming from proton-nucleon interactions, their yield is proportional. The proportionally constant is refered to as the k-factor.

The original well known k-factor value is modified by the multiple scattering, the setup acceptance and by detector and trigger inefficiencies. Using the generators and the GEANT simulation of the spectrometer we have calculated the 'experimental' k-factor value.

In addition, systematic influences due to multiple scattering have been studied and are found to be most important for very small relative momenta ($Q < 2$ MeV/c).

Lastly we have discussed the possibility of using a fast toy model to avoid the lengthy proccesing of Monte Carlo events. However, this option should not be considered for a very precise analysis of the data.

References

[1] B. Adeva, *et al*., Nucl. Instr. and Meth. in Phys. Res. A 515, 467 (2003).

[2] B. Adeva *et al*., Lifetime measurement of $\pi^+\pi^-$ atoms to test low energy QCD predictions, CERN/SPSLC 95-1 (1994); `http://www.cern.ch/DIRAC`.

[3] A. D. Sakharov. Zh. Eksp. Teor. Fiz., 18, 631ff (1948).

[4] L. L. Nemenov, Yad. Fiz. 41, 980 (1985); Sov. J. Nucl. Phys. 41 629 (1985).

[5] R. Lednicky and J. Smolik, private communication.

[6] I. Amirkhanov, I. Puzynin, A. Tarasov, O. Voskresenskaya and O. Zeinalova, Phys. Lett. B 452 155 (1999).

[7] L. Afanasyev, Observation of $\pi^+\pi^-$ atoms, PhD thesis, JINR, Dubna (1997)

[8] Afanasyev L G *et al*. Phys. At. Nucl. 60 938 (1997).

[9] R. Lednický, Proceedings of the HadAtom 99 Workshop, BUTP-99/26, BUHE-99/08 (1999) 7.

[10] Z.K. Silagadze, JETP Lett. **60** (1994) 689.

[11] Uzhinskii V V 1996 JINR preprint E2-96192 Dubna.

B. Andersson *et al.*, Nuclear Physics **B 281** (1987) 289.

B. Nilsson-Almquist and E. Stenlund, *Comp. Phys. Comm* **43** (1987) 387.

[12] C. Schütz and L. Tauscher, The BASEL SFD Y prediction in the DIRAC experiment, DIRAC internal note 2002-04, (2002).

[13] C. Schütz, Detector response simulation for the vertical and horizontal hodoscopes in the DIRAC experiment, DIRAC internal note 2001-07 (2001).

[14] C. Santamarina, PhD thesis: Detection and life time measurement of Pionium in the DIRAC experiment, Appendix C, (2001).

C. Santamarina *et al.*, J. Phys. **B 36**, (2003) 4273.

[15] T.A.Heim, K.Hencken, M.Schumann, D.Trautmann and G.Baur, Proceedings of the HadAtom 01 Workshop 13, `http://www.arxiv.org/ps/hep-ph/0112293`.

[16] The GEANT-DIRAC simmulation program version 2.61, `http://zrelov.home.cern.ch/zrelov/dirac/montecarlo/instruction/instruct26.html`.

[17] Detector and trigger simulation package which is included in the current version of ARIANE 304-24, `http://dirac.web.cern.ch/DIRAC/offlinedocs/SimulData.html`.

[18] ARIANE, the DIRAC Offline software version 304-29, `http://dirac.web.cern.ch/DIRAC/Userguide.html`.

[19] Ch. P. Schütz and L. Tauscher, The BASEL tracking algorithm in the DIRAC experiment, DIRAC internal note 2003-06 (2003).

[20] C. Schütz and L. Tauscher, The behavior of the BASEL extended tracking and the standard ARIANE tracking to $\mathrm{A}_{2\pi}$ Monte Carlo data in the DIRAC experiment, DIRAC internal note 2002-01, (2002).

[21] A. Gorin, et. al. Peak-sensing discriminator for multichannel detectors with cross-talk. NIM A 452, 280-288 (2000).

[22] D. Goldin and L. Tauscher, Scintillating fiber detector efficiency study, DIRAC internal note 2003-02 (2003).

[23] F. Takeutchi, SFD Inefficiencies, Talk given at a DIRAC analysis meeting (2002).

[24] O. Gortchakov, Comparison of Coulomb correlation functions, Talk given at a DIRAC analysis meeting (2003).

[25] MINUIT version 94.1, available from CERN.

[26] Frodesen, Skjeggestad and Tofte, Probability and statistics in particle physics, Universitetsforlaget (1979).